Optica Applicata, Vol. XLIII, No. 1, 2013
DOI: 10.5277/oa130117

Temperature-induced changes in the topography and morphology of C–nPd films deposited on fused silica

RYSZARD DIDUSZKO, EWA KOWALSKA, MIROSŁAW KOZŁOWSKI, ELŻBIETA CZERWOSZ, ANNA KAMIŃSKA

Tele and Radio Research Institute, Ratuszowa 11, 03-450 Warsaw, Poland

*Corresponding author: rydidu@op.pl

Changes in superficial and structural properties in carbonaceous–palladium (C–Pd) films prepared by PVD method, induced by annealing them in an inert atmosphere were studied. C–Pd films with different Pd content in a carbon matrix were investigated. SEM observation after heat treatment showed the agglomeration of palladium nanograins into bigger grains and significant changes in a topography and morphology of C–Pd films. XRD studies confirmed the formation of big (more than 100 nm in diameter) Pd nanograins as a result of the annealing process. FTIR studies showed that C–Pd films from PVD process contained fullerene C_{60} and palladium acetate (films precursors), which were decomposed during the annealing process.

Keywords: carbonaceous–palladium film, PVD, XRD, SEM, FTIR.

1. Introduction

The structure and the composition of carbonaceous–nanopalladium (C–nPd) films, that are new material proposed for hydrogen sensors or hydrogen storage, affect their sensing or storing properties. This type of material can appear in the various structural forms of both components: palladium and carbon matrix. Nanopalladium can be found in the form of nanoparticles, nanowires or nanocrystallites, whereas the carbon matrix can be porous, amorphous carbon or higher ordered nanostructures. The structure of palladium is of a great importance taking into account the hydrogen sensing properties of C–nPd films. There are known several crystalline forms of palladium, palladium-oxide and palladium hydride (PdH_x) phases. Bulk palladium is the *fcc* structure, with the lattice constant $a = 0.3890$ nm. For this *fcc* structure, the diffraction peaks with the largest intensity are observed at 0.2246 and 0.1945 nm, which is ascribed to (111) and (200) lattice planes, respectively. Palladium can also form icosahedral, decahedral or *fcc* nanoclusters depending on the cluster diameter, with the size regime for cluster stability computed by molecular dynamics [1].

The main palladium-oxide phase is palladinite (PdO) which is a tetragonal phase, with the space group *P*42/*mmc* [2], and with the lattice constants: $a = 0.30456$ nm and $c = 0.53387$ nm respectively. Alternative palladium-oxide phases are *fcc*-PdO [3] (space group *Fm*-3*m*, $a = 0.5637$ nm), which is a higher temperature phase, and the PdO_2 phase [4] (space group *P*42/*mnm*, $a = 0.4483$ nm, $c = 0.3101$ nm, tetragonal). Depending on an amount of hydrogen absorption into palladium nanoclusters, the formation of two phases of *fcc* palladium hydrides (α and β) is observed [5]. The α phase (approximately $PdH_{0.015}$), which has the lattice constant close to that of bulk palladium ($a = 0.3890$ nm), occurs at the lower hydrogen concentrations. This phase transforms into the phase ($PdH_{0.6–0.7}$) with the lattice constant of approximately $a = 0.402$ nm, at the higher hydrogen content which depends on a temperature and a pressure of surrounding atmosphere [6].

Adsorption of hydrogen into palladium is a two-step process involving dissociative chemisorption on the Pd surface and subsequent diffusion of hydrogen atoms into the bulk of metal nanograins. Then morphological and structural properties of the films containing palladium in nanosized forms (*e.g.*, size of metal nanograins, their structure and composition) strongly influence their hydrogen sensing properties.

In the last years, it was found that palladium in the form of nanograins causes an improvement in the hydrogen sensing properties. If the Pd particle size approaches the nanoscale dimensions, the probability of the PdH_x forming increases due to a very strong affinity of Pd toward H_2 absorption. This absorption should be reinforced in the nanodimensions sizes due to a high specific surface area of Pd in comparison with the bulk metal [7].

In this paper we present the results of XRD (X-ray diffraction) investigations of carbonaceous–nanopalladium films obtained by PVD (physical vapor deposition) method and by annealing these films at various temperatures in an inert atmosphere. The heat treatment was applied to change the films' structure, topography and morphology. We showed in our previous papers [8–11] that the films obtained by PVD method are composed of palladium nanograins placed in a carbonaceous matrix and that such films are sensitive to hydrogen. Now, we study how the parameters of carbonaceous–nanopalladium films (in the sense of the Pd nanograins size, structure and distribution) are changing with an annealing temperature. Further, we want to use these results for investigations into the influence of these parameters' changes on sensing properties of C–Pd films.

2. Experiment

2.1. Synthesis of C–nPd films

Carbonaceous–nanopalladium films were obtained under dynamic vacuum of 10^{-5} mbar by PVD process. As precursors of these films, fullerene C_{60} (99.98% pure, Aldrich Chemical Co) and palladium(II) acetate $Pd(OAc)_2$ (pure 47% Pd, Fluka) were applied.

T a b l e 1. Temperature of substrates in PVD process and of C–Pd films modified by annealing.

Sample	Temperature of substrate in PVD [°C]	Temperature of annealing process [°C]
Film A, B, C	105, 109, 104	–
Film A1, B1, C1	105, 109, 104	500
Film C2	104	600
Film C3	104	700

Both compounds were evaporated from two separate sources. As the substrate, an unpolished fused silica was used. The initial PVD films were marked here as the films A, B and C according to the different content of Pd that was 25, 36.4 and 46.2 wt%, respectively. Annealed PVD films were marked as A1, B1 and C1–C3 accordingly to the applied temperature. Duration time of annealing for all samples was 30 minutes. In Table 1 temperature parameters of PVD (the substrate's temperature) and annealing process are listed.

2.2. C–Pd films characterization

The characterization of all C–Pd films (A, B and C films) was carried out by the following techniques:

– Scanning electron microscope observations were made by JEOL JSM-7600F field emission scanning microscope, operating at 5 keV incident energy. Two detectors were used: SE (secondary electron) and LABE (low angle backscattered electron). LABE detector shows a contrast composition of analyzed material regarding Z number (Z – atomic number).

– X-ray diffraction studies were carried out on the W1 beamline in Hasylab/DESY synchrotron, using GIXD (grazing incidence X-ray diffraction) measurement geometry, because of thin, low absorption of C–Pd films. Monochromatic synchrotron radiation with a wavelength equal to the line Kα1Cu λ = 1.54056 Å was used.

– FTIR spectra were obtained with ThermoScientific Nicolet iS10 spectrometer using ATR (attenuated total reflectance) technique in the spectral range of 650 to 4000 cm^{-1} at the spectral resolution of 4 cm^{-1}.

3. Results and discussion

3.1. SEM investigation

In Figure 1 we present SEM images of the film C (A and B films look similarly in microscopic images). As one can easily see, the film C covers unpolished fused silica uniformly. In some areas carbon grains are visible, especially in the edge of the substrate. No Pd nanograins on the films' surface were found. In our previous

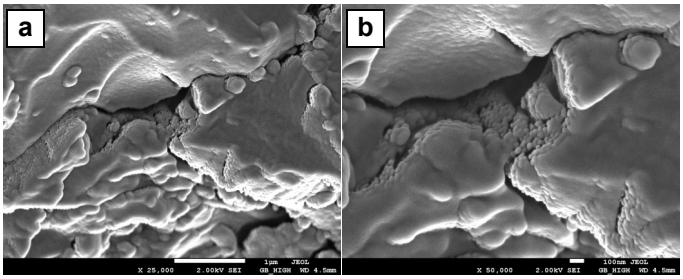

Fig. 1. SEM images of the film C from SE detector with magnifications: ×25 000 (**a**) and ×50 000 (**b**).

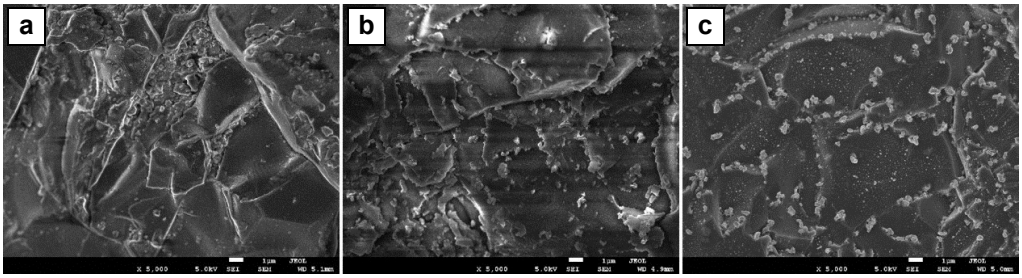

Fig. 2. SEM SE images of the film: C1 (**a**), C2 (**b**) and C3 (**c**).

papers [8, 9], it was shown by high resolution electron transmission microscopy investigations that Pd nanoparticles were embedded in a carbonaceous matrix and their size was about 2 nm.

In Figure 2 SEM images of the films C1, C2 and C3 are shown, respectively. A difference in topography and morphology between the film C and annealed films C1–C3 is clearly visible. After annealing at various temperatures (500, 600 and 700 °C), on the surface of these films many Pd nanograins are found. The sizes and density of distribution of these Pd nanograins change with annealing temperature. SEM images show that with increasing annealing temperature, the size of Pd nanograins increases as well as their density of distribution is greater. Except for very small Pd nanograins with the regular shape for sample C1 annealed at the lowest temperature (diameter is about 10 nm, Fig. 2**a**), big Pd grains with the size up to 500 nm are also observed in samples annealed at higher temperatures (Figs. 2**b** and 2**c**). Especially, these big Pd nanograins appear on the edge of unpolished silica substrate grains. These big nanograins have various shapes due to an agglomeration of small Pd nanograins with different sizes.

A detailed analysis of SE and LABE mode images of annealed samples leads to a conclusion that observed Pd nanograins are surrounded by shells that have probably a carbonaceous character (Fig. 3). From this analysis we can estimate the thickness of such shells as 10–20 nm, depending on the Pd nanograins size. For bigger Pd grains these shells are thicker.

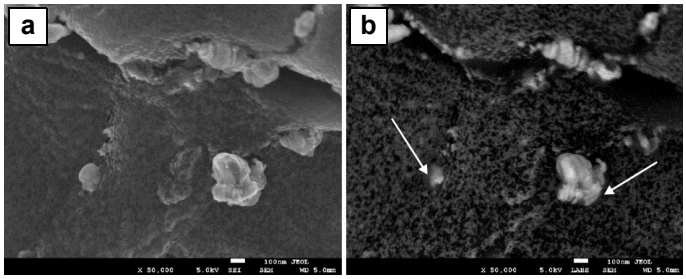

Fig. 3. SEM images of the film C2 from: SE detector (**a**), LABE detector (shells marked by arrows) (**b**).

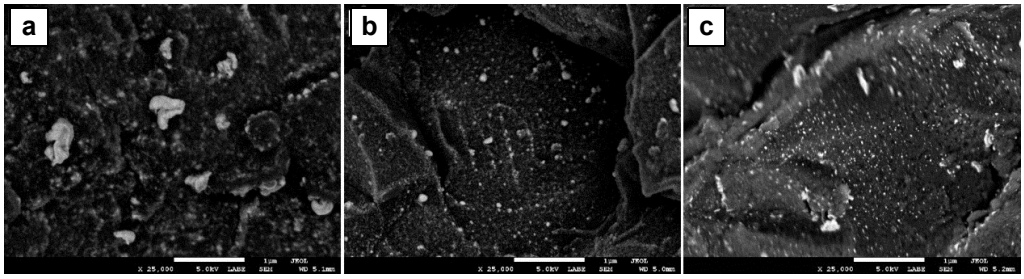

Fig. 4. SEM (LABE) images of the film annealed at 500 °C: A1 (**a**), B1 (**b**), C1 (**c**).

Additionally one can notice that the carbon matrix becomes porous, though in the film C3 annealed at the highest temperature the pores are the smallest.

In Figure 4 SEM images of films A1, B1, C1 with different content of Pd annealed in the same temperature are shown.

3.2. XRD investigation

GIXD diffraction pattern could not be performed for the PVD films: A, B and C, because of too small sizes of Pd nanograins (below a detection limit for the XRD method). Our measurements indicated that all films after the annealing process consisted of palladium nanograins with *fcc* metallic crystalline type of structure. SEM images showed that these Pd nanograins were uniformly distributed in a low-ordered (porous) carbon matrix.

XRD diffraction patterns of the films A1, B1 and C1 are presented in Fig. 5. Diffraction patterns in the range of 2θ angle between 37° and 48° consist of peaks 111 and 200 connected to palladium with *fcc* type of structure. The average sizes of Pd nanocrystallites determined by the Scherrer formula are 34, 32 and 31 nm for A1, B1 and C1 films, respectively. It should be also noticed that 111 and 200 peaks intensity is growing with a decrease in Pd content. This effect can be explained by better ordering in bigger Pd nanocrystallites and higher volume to surface area ratio for sample with the lowest Pd concentration.

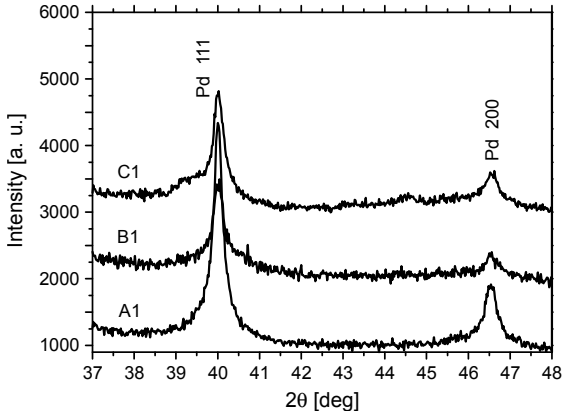

Fig. 5. GIXD diffraction patterns of films A1, B1 and C1 (from annealing process at 500 °C).

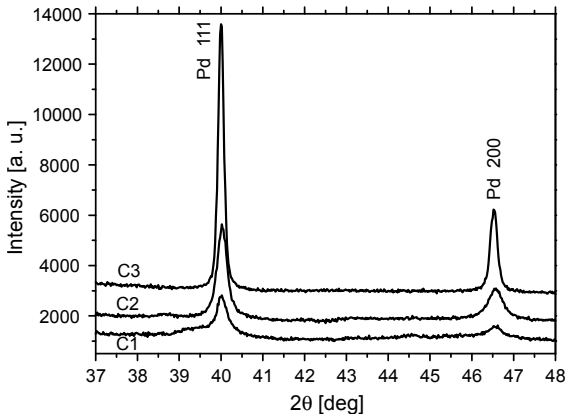

Fig. 6. GIXD diffraction patterns of films C1–C3 annealed at 500, 600 and 700 °C, respectively.

Diffraction patterns of films C1–C3 annealed at 500, 600 and 700 °C are presented in Fig. 6. Lattice constant of Pd crystallites, obtained from diffraction patterns, is similar for all samples and equals $a = 0.3900$ nm and is slightly higher than for the bulk Pd structure. This increase can be connected with the incorporation of oxygen or carbon atoms into Pd lattice and higher density of defects in the structure of Pd particles. Additional EXAFS (extended X-ray absorption fine structure) investigation of such samples should give an answer to a question on the kind of incorporated atoms.

In the case of films C1–C3 the average size of Pd nanograins increases with increasing the annealing temperature and is 31, 32 and 54 nm, respectively (obtained from the Scherrer formula). It should be noticed that the crystallite's size is not equivalent to the size of nanograins observed in SEM images. Observed by SEM, Pd nanograins not only are surrounded by carbonaceous shells but often they also consist of many nanocrystallites forming a big Pd grain due to the agglomeration process. Generally SEM and GIXD results show the similar tendency.

The intensity of 111 and 200 peaks arises with annealing temperature, what could be connected with better ordering in the crystallites. The volume to surface area ratio is also bigger for samples annealed at the highest temperature, and then the disorder connected with the defects formation on grains border is lower.

3.3. FTIR investigation

FTIR spectra of sample C obtained in PVD process as well as samples C1–C3 annealed at 500, 600 and 700 °C are shown in Fig. 7. In FTIR spectrum of film C we found bands connected with the presence of palladium acetate, fullerene C_{60} and fused silica substrate. The narrow band at a wavenumber of 1182 cm^{-1} is associated with the C_{60} pentagon asymmetric deformation [12]. Broadbands placed at 1593 and 1422 cm^{-1} are assigned to asymmetric and symmetric stretching vibrations of C–O bond in the carboxylate groups (CH_3COO^-), while bands at wavenumbers of 1347 and 697 cm^{-1} are connected with bending vibrations of $-CH_3$ group in palladium acetate molecules [13]. We can deduce that the precursors of the film C have not decomposed completely during PVD process. No peaks attributed to palladium acetate and fullerene in obtained GIXD diffraction pattern of this sample are probably connected with lack of the order in the structure of C_{60} and $Pd(OAc)_2$ or too small diameters of these grains. In FTIR spectrum of sample C, the bands originating from fused silica substrate are also visible. Two bands assigned to symmetric and asymmetric stretching vibrations of Si–O bonding are placed at 987 and 786 cm^{-1} [14].

In FTIR spectrum of sample C1 annealed in the lowest temperature (500 °C) besides substrate characteristic bands, we can find only a band assigned to fullerene molecules vibrations. It means complete decomposition of palladium acetate during the annealing process. It is consistent with our results of thermogravimetric studies of

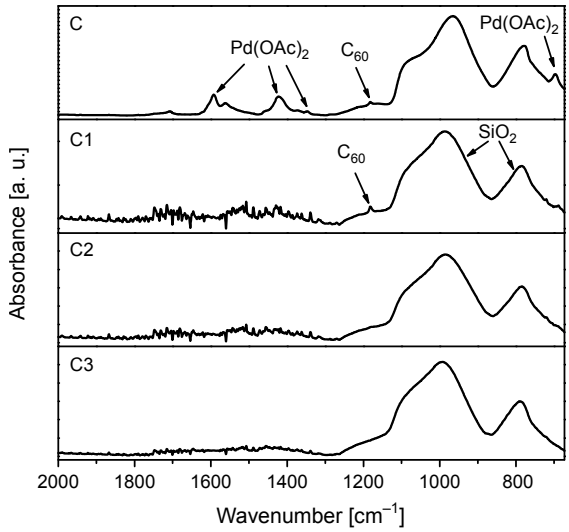

Fig. 7. FTIR spectra of film C and films C1–C3 annealed at 500, 600 and 700 °C.

similar C–Pd samples [11]. The formation of palladium nanograins from $Pd(OAc)_2$ is confirmed by SEM and GIXD investigations of annealed films (Figs. 2 and 5). Lack of a fullerene characteristic band in FTIR spectra of C2 and C3 samples means its decomposition during annealing at higher temperatures.

4. Conclusions

The comparison of SEM and GIXD results allows for a conclusion that films with highest content of Pd and annealed at lowest temperature of 500 °C have the smallest and most densely distributed palladium nanograins, what could be most advantageous for hydrogen detection or storage because of the rate of dissolution of hydrogen in such small palladium grains. FTIR results show that precursors of C–Pd films present in PVD samples are decomposed during the annealing process. An increase in annealing temperature leads to a formation of big Pd nanograins (up to 0.5 μm) due to the agglomeration process. This agglomeration process gives different results when the initial film contains various Pd content. It was stated that for the lowest Pd content annealing at the same temperature causes the growth of bigger grains than for samples containing more of palladium. The porosity of carbonaceous matrix in annealed samples, which is highest for lowest Pd content, plays also a role in this process dynamics.

We can assume that a new kind of C–Pd films annealed in an inert atmosphere could be used as active layers in hydrogen detection or storage. On the annealed films' surface, big Pd nanograins appear and carbon matrix changes into a porous material. Such surface changes could affect a faster response and can be sensitive to hydrogen content in gas atmosphere.

Acknowledgments – This work was supported by the European Regional Development Fund within the Innovative Economy Operational Programme 2007–2013 (project No. UDA-POIG.01.03.01-14-071/08-07) as well as by COST action (No. 577/N-COST/20009/0).

References

[1] SCHEBARCHOV D., HENDY S.C., *Solid-liquid phase coexistence and structural transitions in palladium clusters*, Physical Review B **73**(12), 2006, article 121402(R).
[2] *International Tables of X-ray Crystallography*, IUCr, vol. A.
[3] KUMAR J., SAXENA R., *Formation of NaCl- and Cu_2O-type oxides of platinum and palladium on carbon and alumina support films*, Journal of the Less Common Metals **147**(1), 1989, pp. 59–71.
[4] SHAPLYGIN I.S., Russian Journal of Inorganic Chemistry **23**, 1978, p. 488.
[5] PEARSON W.B., *A Handbook of Lattice Spacings and Structures of Metals and Alloys*, Vol. 2, Pergamon Press.
[6] MAELAND A.J., GIBB T.R.P., *X-ray diffraction observations of the Pd–H_2 system through the critical region*, Journal of Physical Chemistry **65**(7), 1961, pp. 1270–1272.
[7] LEWIS F.A., *The Palladium–Hydrogen System*, Academic Press, London, 2008, p. 1967.
[8] CZERWOSZ E., DIDUSZKO R., DŁUŻEWSKI P., KĘCZKOWSKA J., KOZŁOWSKI M., RYMARCZYK J., SUCHAŃSKA M., *Properties of Pd nanocrystals prepared by PVD method*, Vacuum **82**(4), 2007, pp. 372–376.

[9] CZERWOSZ E., DŁUŻEWSKI P., KĘCZKOWSKA J., KOZŁOWSKI M., SUCHAŃSKA M., WRONKA H., *Palladium nanocrystals and their properties*, Materials Science – Poland **26**(1), 2008, pp. 119–125.

[10] MOLENDA K., KAMIŃSKA A., KRAWCZYK S., KOZŁOWSKI M., CZERWOSZ E., WRONKA H., *Resistance changes of carbon–palladium films obtained by PVD for sensor's applications*, Proceedings of SPIE **8008**, 2011, article 800821.

[11] KOWALSKA E., CZERWOSZ E., KAMIŃSKA A., KOZŁOWSKI M., *Investigation of Pd content in C–Pd films for hydrogen sensor applications*, Journal of Thermal Analysis and Calorimetry **108**(3), 2012, pp. 1017–1023.

[12] BYSZEWSKI P., KLUSEK Z., *Some properties of fullerenes and carbon nanotubes*, Opto-Electronics Review **9**(2), 2001, pp. 203–210.

[13] FANG Q., HE G., CAI W.P., ZHANG J.-Y., BOYD I.W., *Palladium nanoparticles on silicon by photo--reduction using 172 nm excimer UV lamps*, Applied Surface Science **226**(1–3), 2004, pp. 7–11.

[14] SAIKIA B.J., PARTHASARATHY G., SARMAH N.C., *Fourier transform infrared spectroscopic estimation of crystallinity in SiO_2 based rocks*, Bulletin of Materials Science **31**(5), 2008, pp. 775–779.

Received May 25, 2012
in revised form August 8, 2012